Geophysical Research Letters

RESEARCH LETTER
10.1029/2023GL105084

Key Points:

- Basin-averaged rapid intensification magnitude over the western North Pacific is significantly related to the West Pacific teleconnection
- Strong increases (weak decreases) in rapid intensification magnitude occur at low (high) latitudes during a positive West Pacific phase
- West Pacific teleconnection controls interannual changes in rapid intensification magnitude mainly by modulating vertical wind shear

Supporting Information:

Supporting Information may be found in the online version of this article.

Correspondence to:

J. Song,
songjinjie@qq.com

Citation:

Song, J., Klotzbach, P. J., Wei, N., & Duan, Y. (2023). What controls the interannual variation in rapid intensification magnitude of western North Pacific tropical cyclones? *Geophysical Research Letters*, *50*, e2023GL105084. https://doi.org/10.1029/2023GL105084

Received 19 JUN 2023
Accepted 6 OCT 2023

What Controls the Interannual Variation in Rapid Intensification Magnitude of Western North Pacific Tropical Cyclones?

Jinjie Song[1,2], Philip J. Klotzbach[3], Na Wei[1], and Yihong Duan[2]

[1]Nanjing Joint Institute for Atmospheric Sciences, Chinese Academy of Meteorological Sciences, Nanjing, China, [2]State Key Laboratory of Severe Weather, Chinese Academy of Meteorological Sciences, Beijing, China, [3]Department of Atmospheric Science, Colorado State University, Fort Collins, CO, USA

Abstract This study investigates the interannual variability of rapid intensification (RI) magnitude of western North Pacific (WNP) tropical cyclones. There is a significant correlation between basin-averaged RI magnitude during July–November and the simultaneous Western Pacific (WP) teleconnection index from 1982 to 2021. RI magnitude is, on average, larger (smaller) in positive (negative) WP phases. During a positive WP, RI magnitude changes exhibit a southwest-northeast dipolar pattern, with significant increases over the southwestern quadrant of the WNP and weak decreases over the northern part of the WNP. The WP teleconnection relates to RI magnitude primarily through modulation of 850–200-hPa vertical wind shear, with less influence from 850-hPa relative vorticity. The changes in these two dynamic conditions can be linked to WP-induced circulation anomalies at lower and upper levels. Our results highlight that different contributors may be responsible for changes in WNP RI occurrence and RI magnitude.

Plain Language Summary Rapid intensification (RI) is commonly recognized as a sharp increase in tropical cyclone (TC) intensity over a short duration, posing a significant challenge for operational TC forecasting. Given concerns about climate change and its impacts on TC activity, there has been an increasing focus on temporal variations of RI. Unlike most previous publications investigating changes in RI occurrence, this study focuses on the interannual variability of RI magnitude, defined as the TC intensity increase during the 24-hr RI stage. There is a significant interannual correlation between basin-averaged RI magnitude over the western North Pacific during July–November and the simultaneous Western Pacific (WP) teleconnection index from 1982 to 2021. During a positive WP, RI magnitude significantly increases over the southwestern quadrant of the basin because of significantly reduced 850–200-hPa vertical wind shear. RI magnitude weakly decreases over the northern part of the basin, likely linked to slightly enhanced vertical wind shear. These vertical wind shear changes can be further linked to WP-induced circulation anomalies at lower and upper levels. Our results highlight the dominant (lesser) role of vertical wind shear (850-hPa relative vorticity) in controlling the interannual variation of RI magnitude over the western North Pacific.

1. Introduction

Rapid intensification (RI) is recognized as a sharp increase in tropical cyclone (TC) intensity over a short duration. RI prediction still poses significant challenges for operational TC forecasting, owing to an incomplete understanding of the physical mechanisms responsible for RI (DeMaria et al., 2021; Knaff et al., 2018). Both internal factors and environmental conditions can influence RI (Hendricks et al., 2010). Internal factors are related to the TC's thermodynamic and dynamic structure as well as their spatiotemporal variations, which can sometimes be modulated by changes in the large-scale environment. RI-favoring environmental conditions include large maximum potential intensity (MPI), high tropical cyclone heat potential (TCHP), a moist lower-to-middle troposphere, low vertical wind shear (VWS), an anomalous low-level cyclonic circulation and upper-level divergent flow (Kaplan & DeMaria, 2003; Kaplan et al., 2010; Knaff et al., 2018; Shu et al., 2012; Wang & Zhou, 2008).

The western North Pacific (WNP) has the most frequent RI occurrences of any global TC basin on an annually-averaged basis (Lee et al., 2016). Several studies (e.g., Guo & Tan, 2021; Song et al., 2022; Wang & Zhou, 2008) have investigated interannual changes in WNP RI activity. Wang and Zhou (2008) reported a significant simultaneous interannual relationship between WNP RI occurrence and El Niño-Southern Oscillation (ENSO). Compared with La Niña years, the mean frequency of WNP RI events was notably higher in El Niño

years, while the average location of RI occurrence shifted equatorward and eastward. This shift is a result of an RI-favorable environment with an enhanced and southeastward-extended monsoon trough over the WNP in El Niño years (Wang & Zhou, 2008). When considering different ENSO flavors and different TC seasons, Guo and Tan (2021) found that RI number during the early season (April–June) in eastern Pacific (EP) El Niño years was relative lower than in either central Pacific (CP) El Niño or La Niña. During the peak season (July–September), the mean RI onset position significantly migrated poleward in La Niña years, while it weakly shifted southward and northward in EP El Niño years and CP El Niño years, respectively. During the late season (October–December), the mean RI onset position shifted significantly westward in both EP El Niño and La Niña years. These shifts were further attributed to corresponding changes in the thermal state of the upper ocean, mid-tropospheric relative humidity and VWS (Guo & Tan, 2021). In addition, Song et al. (2022) showed a significant inverse correlation between WNP RI number and the Antarctic Oscillation (AAO). During positive (negative) AAO years, RI occurrence was significantly suppressed (enhanced) over most of the WNP, except the South China Sea (SCS). The AAO-induced changes were primarily driven by anomalous changes in the WNP low-level circulation (Song et al., 2022).

Most RI-related publications have focused on the frequency of WNP RI occurrence. Recently, several studies have investigated changes related to RI magnitude, as measured by the 24-hr TC intensity change during the RI stage (Balaguru et al., 2018; Li et al., 2023; Song et al., 2020). Song et al. (2020) showed that there was a significant increasing trend in WNP RI magnitude since 1979, mainly resulting from increased sea surface temperatures (SSTs) and ocean heat content. However, changes in WNP RI number were not significant during the same period.

Li et al. (2023) examined WNP RI activity in 1998 and 2010. They found that although RI occurrence frequency was significantly lower than the 1979–2020 average in both years, RI magnitude was the third highest in 1998 but the lowest in 2010. They attributed the high RI magnitude in 1998 to increased ocean warming coupled with an unstable atmosphere, while the low RI magnitude in 2010 was linked to decreased low-level relative vorticity. The above studies imply that changes in RI magnitude are driven by potentially different atmospheric/oceanic factors than RI number.

It is still unknown what controls changes in WNP RI magnitude on interannual timescales. Given the modulation of WNP RI occurrence by ENSO and the AAO (e.g., Song et al., 2022; Wang & Zhou, 2008), we investigate what climate modes can influence WNP RI magnitude via correlations of WNP RI magnitude to global SSTs and 500-hPa geopotential heights. Based on the spatial pattern of the correlation between WNP RI magnitude and global 500-hPa geopotential heights (Figure 1e), we investigate the statistical linkage between WNP RI magnitude and the large-scale environment as influenced by the Western Pacific (WP) teleconnection (Barnston & Livezey, 1987).

The positive phase of the WP teleconnection is characterized by anomalously high heights off the coast of Japan and anomalously low heights in the subtropical WNP, while the negative phase of the WP teleconnection is characterized by anomalies of the opposite sign. These changes result in shifts in the position of the East Asian jet stream, which modulate large-scale environmental factors that either favor or disfavor TCs.

The remainder of this study is organized as follows. Section 2 introduces the TC and environmental data sets employed as well as the analysis methodology. Section 3 displays spatiotemporal variations in WNP RI occurrence and magnitude as driven by the WP teleconnection. Section 4 shows how the WP teleconnection modulates several environmental variables. Section 5 discusses the influences of several environmental factors on RI occurrence and magnitude. This study concludes with a summary in Section 6.

2. Data and Methods

This study uses the 6-hourly TC best track data from the Joint Typhoon Warning Center provided by the International Best Track Archive for Climate Stewardship (IBTrACS) (v04r00), including TC central position and maximum 1-m sustained wind (V_{max}) over the WNP (north of the equator and 100°E–180°). Only the recent period of 1982–2021 is considered, when TC intensity estimates are of higher quality given the near-global coverage of geostationary satellites starting in 1982 (Moon et al., 2019). Consistent with previous RI-related studies (Kaplan & DeMaria, 2003; Kaplan et al., 2010; Knaff et al., 2018; Shimada et al., 2020; Shu et al., 2012), an RI event is identified as a 24-hr V_{max} (ΔV_{24}) intensification of at least 30 kt over water, approximately corresponding to the 95th percentile of ΔV_{24} for all TC cases. Here, starting from the first 6-hr point (t_0) of the TC, a ΔV_{24} ($V_{max}[t_0 + 24\ hr] - V_{max}[t_0]$) is calculated for every 6-hr point. Note that RI events defined here are counted in 6-hr intervals when the above criteria are satisfied. Each RI event has a duration of 24 hr, with one consecutive RI

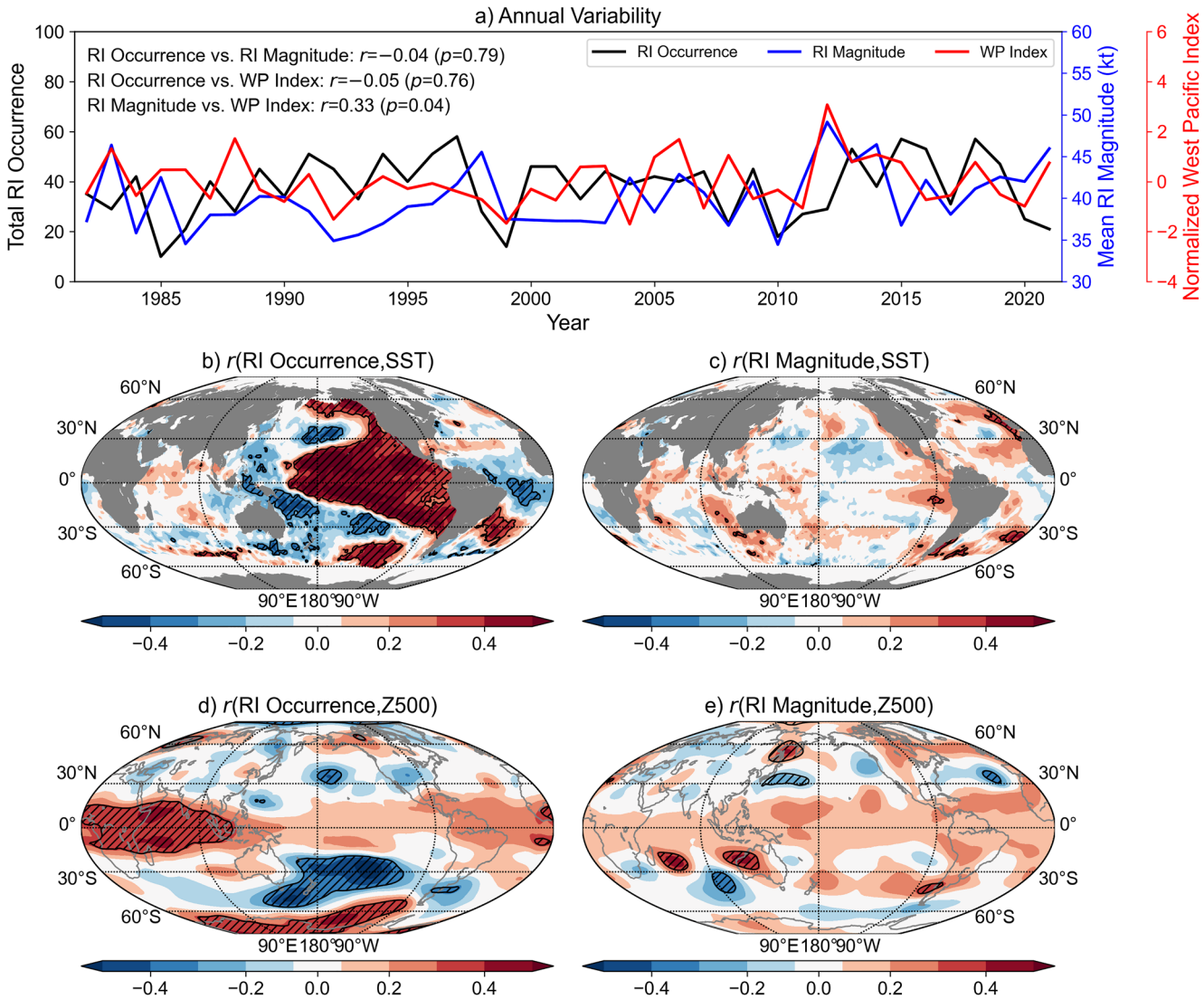

Figure 1. (a) Total WNP RI occurrence, mean RI magnitude and the WP index during JASON from 1982 to 2021. (b–e) Spatial distributions of correlations for (b) RI occurrence versus SST, (c) RI magnitude versus SST, (d) RI occurrence versus 500-hPa geopotential height and (e) RI magnitude versus 500-hPa geopotential height during 1982–2021. Hatched areas denote correlations significant at the 0.05 level.

period of a TC lasting more than 24 hr being recognized as multiple RI events. In other words, one RI event will overlap with its preceding or following event if an RI period longer than 24-hr occurs. Our results are not significantly changed if RI events are identified in 24-hr intervals (figures not shown). Similar to previous publications (Balaguru et al., 2018; Li et al., 2023; Song et al., 2020), RI magnitude is defined as ΔV_{24} during the 24-hr RI stage, so by definition its lower limit is 30 kt. We focus on WNP RI activity during July–November (JASON), which includes the majority (84%) of RI events that occur over the entire year (Ge et al., 2018; Wang & Zhou, 2008).

Six large-scale environmental factors potentially influencing RI activity are considered in this study, including maximum potential intensity (MPI), tropical cyclone heat potential (TCHP), 700–500-hPa relative humidity, 850–200-hPa VWS, 850-hPa relative vorticity and 200-hPa divergence (Fudeyasu et al., 2018; Knaff et al., 2018; Shu et al., 2012). Specifically, these variables are first calculated from monthly data and then are averaged for the full JASON season. Our results are not significantly different if these variables are computed from JASON-averaged large-scale fields (figures not shown). We calculate MPI using the formula of Emanuel (1988):

$$\mathrm{MPI} = \sqrt{\frac{C_k}{C_d}\frac{\mathrm{SST} - T_0}{T_0}(k^* - k)}, \quad (1)$$

where T_0 is the temperature of the outflow, k^* is the saturation enthalpy of air at the sea surface, k is the enthalpy of the boundary layer air overlying the surface, and C_k and C_d are the surface exchange coefficients of enthalpy and momentum, respectively. TCHP is a measure of ocean heat content that is warmer than 26°C (DeMaria et al., 2005) and is computed as:

$$\mathrm{TCHP} = c_p \rho \int_{D_{26}}^{0} [t(z) - 26] dz, \tag{2}$$

where c_p is the heat capacity of water, ρ is the density of water, D_{26} is the depth of the 26°C isotherm, and $t(z)$ is the water temperature at depth z.

Monthly mean atmospheric variables are derived from the fifth generation European Centre for Medium-Range Weather Forecasts (ECMWF) reanalysis of the global climate (ERA5) with a resolution of 0.25° × 0.25°. Monthly mean SST data over a 1° × 1° grid are from the Hadley Centre Sea Ice and Sea Surface Temperature data set (HadISST; Rayner et al., 2003). Monthly ocean subsurface temperature profiles over a 0.25° × 0.25° grid are from the control member of the ECMWF Ocean Reanalysis System 5 (ORAS5). HadISST and ERA5 provide the primary forcing fields for ORAS5 (Zuo et al., 2019), leading to physical consistency between our data sets. July–November averages of both the Niño-3.4 SST anomaly and the AAO index are obtained from NOAA's Earth System Research Laboratory Physical Sciences Division. Following Wallace and Gutzler (1981), the WP teleconnection index (hereafter WP index) is defined as:

$$\mathrm{WP} = \frac{1}{2}\left[z^*(60°\mathrm{N}, 155°\mathrm{E}) - z^*(30°\mathrm{N}, 155°\mathrm{E})\right], \tag{3}$$

where z^* represents monthly normalized 500-hPa geopotential height derived from ERA5. We also use 6-hourly environmental parameters extracted from the Statistical Typhoon Intensity Prediction Scheme (STIPS; Knaff et al., 2005) developmental data between 1990 and 2020.

The significance levels (p) of correlation coefficients (r), partial correlation coefficients and the differences in means between two samples are estimated using a two-tailed Student's t-test. In evaluating statistical significance, the effective sample size proposed by Trenberth (1984) is applied to minimize the influence of autocorrelation.

3. Changes in RI Number and RI Magnitude Associated With WP

Figure 1a displays interannual variations of RI number and RI magnitude over the WNP during JASON from 1982 to 2021. The correlation coefficient between RI number and RI magnitude is −0.04 ($p = 0.79$), meaning that they are linearly independent. The detrended correlation coefficient is also insignificant ($r = -0.09$; $p = 0.56$). The spatial distribution of the correlation between RI number and simultaneous SST is characterized by an El Niño-like pattern, with significant positive correlations extending from the equatorial central Pacific to the equatorial and extratropical eastern Pacific in both hemispheres and significant negative correlations occurring over the equatorial western Pacific (Figure 1b). This confirms the relationship between WNP RI number and ENSO as found in Wang and Zhou (2008). However, there are almost no significant correlations between RI magnitude and simultaneous SST (Figure 1c). Consequently, it is possible that the annual variability of WNP RI magnitude is not driven by known SST modes (e.g., ENSO).

The spatial distribution of the correlation between RI number and the simultaneous 500-hPa geopotential height shows significant positive correlations in the Southern Hemisphere polar regions and significant negative correlations over the extratropical South Pacific (Figure 1d). This pattern is similar to a negative AAO pattern, consistent with the inverse relationship between RI number and the AAO shown in Song et al. (2022). By comparison, significant correlations between RI magnitude and simultaneous 500-hPa geopotential height are observed near Japan (Figure 1e). There is a dipole structure with positive values near 60°N and negative values near 30°N, characteristic of a positive phase of the WP teleconnection.

Choi and Moon (2012) found that TCs occurred more frequently in boreal summer during positive WP phases than during negative WP phases. Positive WP phases favored TCs recurving into the northeastern part of the WNP. Here, we find a significant interannual linkage between WNP RI magnitude and the WP index ($r = 0.33$; $p = 0.04$) (Figure 1a). This linkage remains significant when the long-term linear trends in both indices are

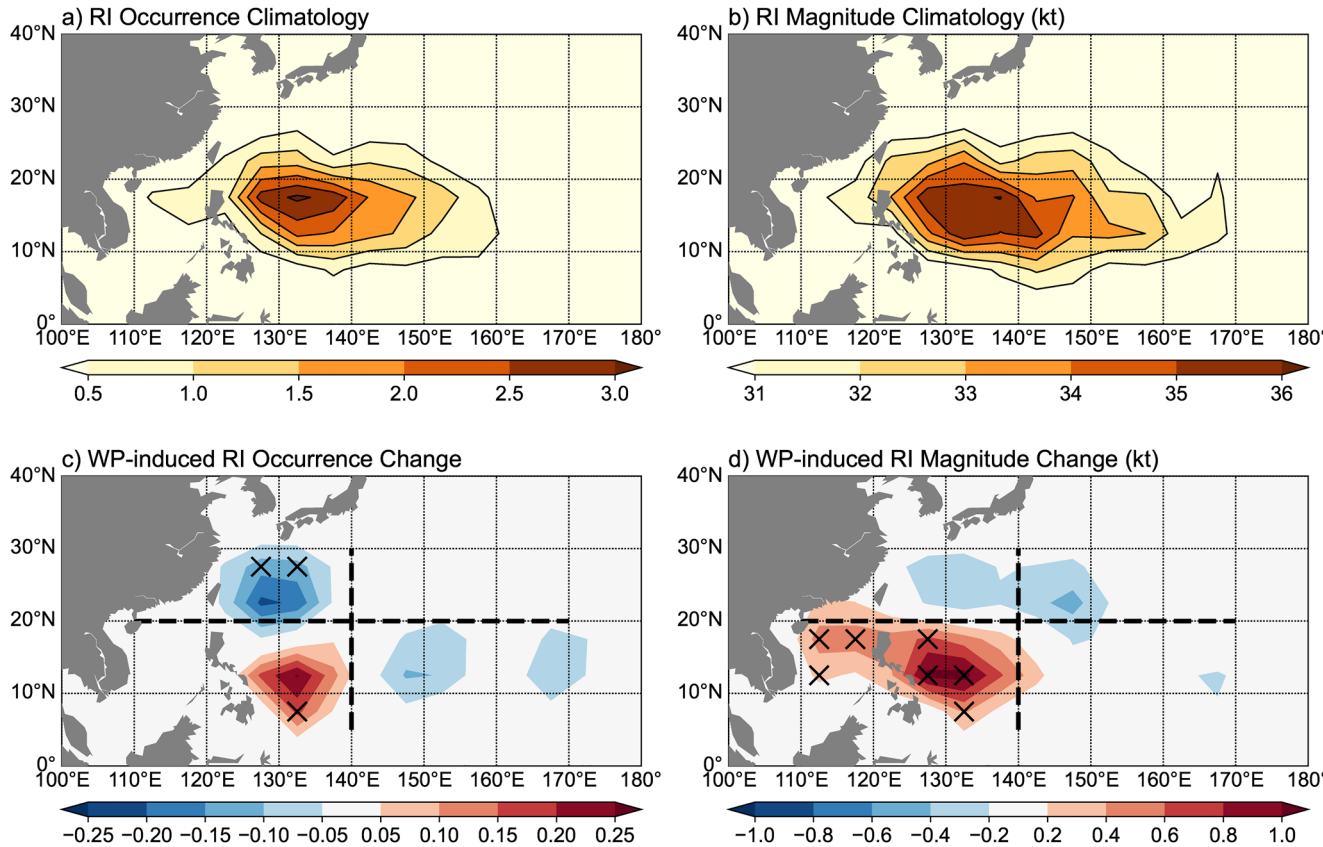

Figure 2. (a, b) Climatological (1982–2021) JASON (a) RI occurrence and (b) RI magnitude over the WNP. (c, d) Regressions of (c) RI occurrence and (d) RI magnitude onto the WP index during 1982–2021. Black crosses denote regressions significant at the 0.05 level. The black dashed lines denote the four WNP quadrants.

removed ($r = 0.32$; $p = 0.04$). Moreover, the correlation coefficient remains nearly unchanged when the linear influence of ENSO or the AAO is excluded. The lack of change in correlation is primarily due to the insignificant simultaneous correlations between the WP index and the Niño-3.4 SST anomaly ($r = 0.11$; $p = 0.52$) and between the WP index and the AAO index ($r = 0.01$; $p = 0.95$). By contrast, there is a weak and insignificant correlation between RI number and the WP index ($r = -0.05$; $p = 0.76$). There is also a weak correlation after removing the trends ($r = -0.06$; $p = 0.71$). These results indicate that there are distinct modulations of RI number and RI magnitude by the WP teleconnection.

Figures 2a and 2b display the 40-yr climatological (1982–2021) distributions of RI occurrence and RI magnitude over the WNP during JASON, by counting 6-hr RI events and calculating their mean magnitude over individual 5° × 5° grids. Similar spatial features are observed, with more RI occurrences and higher RI magnitudes east of the Philippines. Nonetheless, Figures 2c and 2d show different responses of RI occurrence and RI magnitude to the WP teleconnection. Note that changes in both RI occurrence and RI magnitude associated with the WP are not significantly altered when the effect of ENSO or the AAO is removed (Figure S1 in Supporting Information S1). WP-induced changes in RI occurrence between 120°E and 140°E are of a greater magnitude than those over other parts of the WNP (Figure 2c). During a positive WP, there is a south-north dipolar pattern in RI occurrence, with significantly enhanced RI occurrences over the southwestern WNP (SWWNP; south of 20°N, west of 140°E) and significantly suppressed RI occurrences over the northwestern WNP (NWWNP; north of 20°N, west of 140°E). Given the comparable magnitudes of these changes in RI occurrence, the basinwide RI number changes little during different WP phases.

By comparison, WP-induced changes in RI magnitude are characterized by a southwest-northeast dipolar structure (Figure 2d). During a positive WP, significant RI magnitude increases occur over the SWWNP, extending from the Philippine Sea to the SCS, and are much larger than the region with significant RI occurrence increases. Most of the RI magnitude decreases occur over the northern WNP (NWNP; north of 20°N), particularly

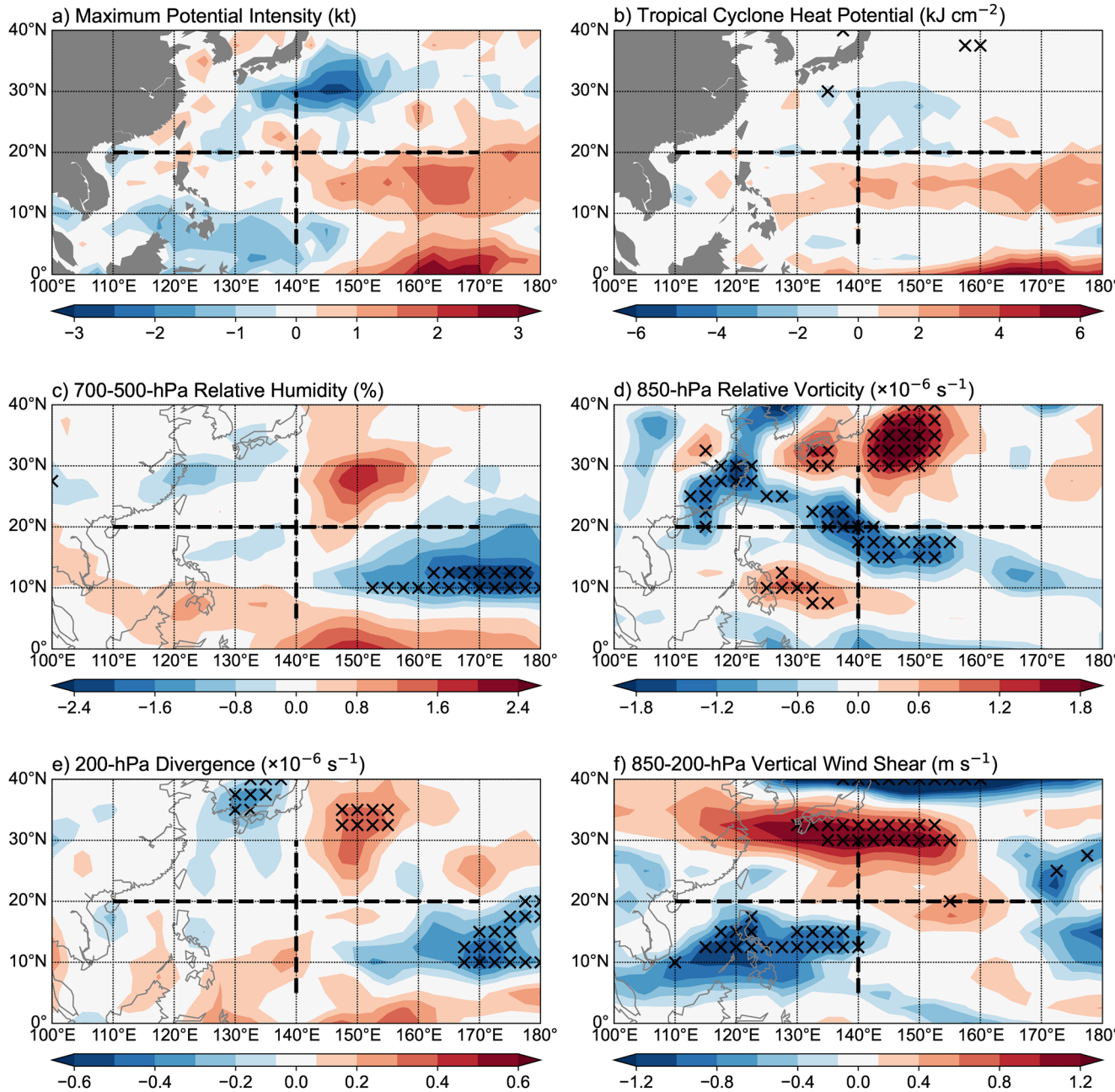

Figure 3. Regressions of environmental variables on the WP index from 1982 to 2021, including (a) MPI, (b) TCHP, (c) 700–500-hPa relative humidity, (d) 850-hPa relative vorticity, (e) 200-hPa divergence, and (f) 850–200-hPa vertical wind shear. Black crosses denote regressions significant at the 0.05 level. The black dashed lines denote the four WNP quadrants.

south of Japan. These decreases are insignificant and much weaker than the RI magnitude increases over the SWWNP. These results imply that during different WP phases, SWWNP RI magnitude changes dominate variations in basin-averaged RI magnitude. Moreover, RI occurrence and RI magnitude change differently over some parts of the WNP, particularly over the NWNP, when the same environmental changes induced by the WP teleconnection are considered.

4. Environmental Changes Associated With WP

Compared with internal dynamics, environmental conditions controlled by climate variability play a dominant role in influencing RI activity on interannual timescales (Hong & Wu, 2021). Figure 3 displays changes in

environmental variables associated with the WP teleconnection. During a positive WP, increased MPIs concentrate over the southeastern WNP (SEWNP; south of 20°N, east of 140°E), while decreased MPIs occur over most of the other quadrants of the WNP (Figure 3a). Increased TCHPs develop near the equator and within the latitudinal belt of 10°–20°N, while decreased TCHPs occur over the NWNP (Figure 3b). We do not find any other significant large-scale WP-induced changes in MPI and TCHP (Figures 3a and 3b). During a positive WP, significant decreases in 700–500-hPa relative humidity are concentrated over the SEWNP, while weak decreases in relative humidity are observed over other sub-regions of the WNP (Figure 3c). These results indicate that the WP teleconnection appears to play a minor role in modulating thermodynamic conditions influencing RI activity.

There are larger regions with significant WP-induced changes in dynamic variables relative to thermodynamic variables (Figures 3d–3f). During a positive WP, significant increases in 850-hPa relative vorticity are found over the SWWNP, particularly southeast of the Philippines. Weak decreases in relative vorticity are distributed along the belt extending from the NWWNP to the SEWNP. This distribution likely explains the south-north dipolar pattern of WP-induced changes in RI occurrence (Figure 2c). By comparison, despite significant decreases in 200-hPa divergence near the dateline over the central Pacific, there are only weak changes in 200-hPa divergence over other parts of the tropical WNP (Figure 3e). Additionally, 850–200-hPa VWS is significantly reduced over the SWWNP, including the SCS and the area east of the Philippines, corresponding to significant RI magnitude increases (Figure 3f). Only insignificant VWS increases occur over most of the NWNP, consistent with weak decreases in RI magnitude.

In summary, during a positive WP, there are significantly increased 850-hPa relative vorticity and significantly decreased 850–200-hPa VWS over the SWWNP, associated with significant increases in both RI occurrence and RI magnitude. By comparison, there is significantly decreased relative vorticity but weakly increased VWS over the NWWNP, with significant RI occurrence decreases and weak decreases in RI magnitude. During a positive WP, the spatial distribution of RI magnitude changes is more like that of VWS changes than that of vorticity changes. Consequently, it appears that changes in relative vorticity play only a minor role in interannual variations in WNP RI magnitude. This finding is discussed further in Section 5.

Given that dynamic variables likely play a more important role in influencing RI activity over the SWWNP and NWWNP than thermodynamic variables do, Figure 4 displays how the WP teleconnection modulates 850-hPa relative vorticity and 850–200-hPa VWS. Climatologically, the SWWNP corresponds to the monsoon trough region, characterized by low-level southwesterly flow (Figure 4a). The NWWNP is located along the western edge of the western Pacific subtropical high and is associated with low-level southerly flow. At upper levels, both the SWWNP and the NWWNP are located over the southeastern part of the South Asian high, characterized by northeasterly flow (Figure 4b).

Figure 4c shows that a positive WP is characterized by a dipolar structure in the 850-hPa flow at mid-to-high latitudes, with an anomalous anticyclone centered at 55°N, 170°E and an anomalous cyclone centered at 35°N, 145°N. This cyclone and another three cyclonic/anticyclonic circulations at relatively smaller spatial scales consist of a large-scale deformation pattern at lower-to-mid latitudes (Figure 4c). One anomalous cyclone centered at 10°N, 135°E occurs over the SWWNP, providing positive vorticity anomalies. By comparison, the NWWNP is located near the horizontal ridge of one anomalous anticyclone centered at 25°N, 115°E, inducing negative vorticity anomalies.

The dipolar flow pattern of the WP extends from lower levels to upper levels, with no obvious vertical tilting (Figure 4d). During a positive WP, the anomalous cyclone centered at 35°N, 145°N influences a much larger area at 200 hPa than at 850 hPa, inducing anomalous upper-level westerlies over most of the tropical WNP. Over the SWWNP, there are significant anomalous westerlies at 200 hPa, opposing the climatological northeasterlies, which implies a significant deceleration of the 200-hPa winds. By comparison, only weak wind anomalies are observed at 850 hPa. These weak wind anomalies are of a much smaller magnitude than the 200-hPa wind anomalies (Figure 4c). These results mean that significant VWS decreases over this area are primarily caused by significant 200-hPa wind decreases. Over the eastern part of the SWWNP (east of 130°E), the anomalous cyclonic circulation at 850 hPa is in the same direction as the climatological winds (Figure 4c). The deceleration of 200-hPa winds and the acceleration of 850-hPa winds jointly lead to VWS decreases in this region. Over most of the NWWNP, anomalous westerlies oppose climatological easterlies at both 850 and 200 hPa, with the magnitude of 850 hPa wind anomalies being slightly greater than the 200 hPa wind anomalies (Figures 4c and 4d). The greater reduction in 850-hPa winds than 200-hPa winds induces 850–200-hPa VWS increases.

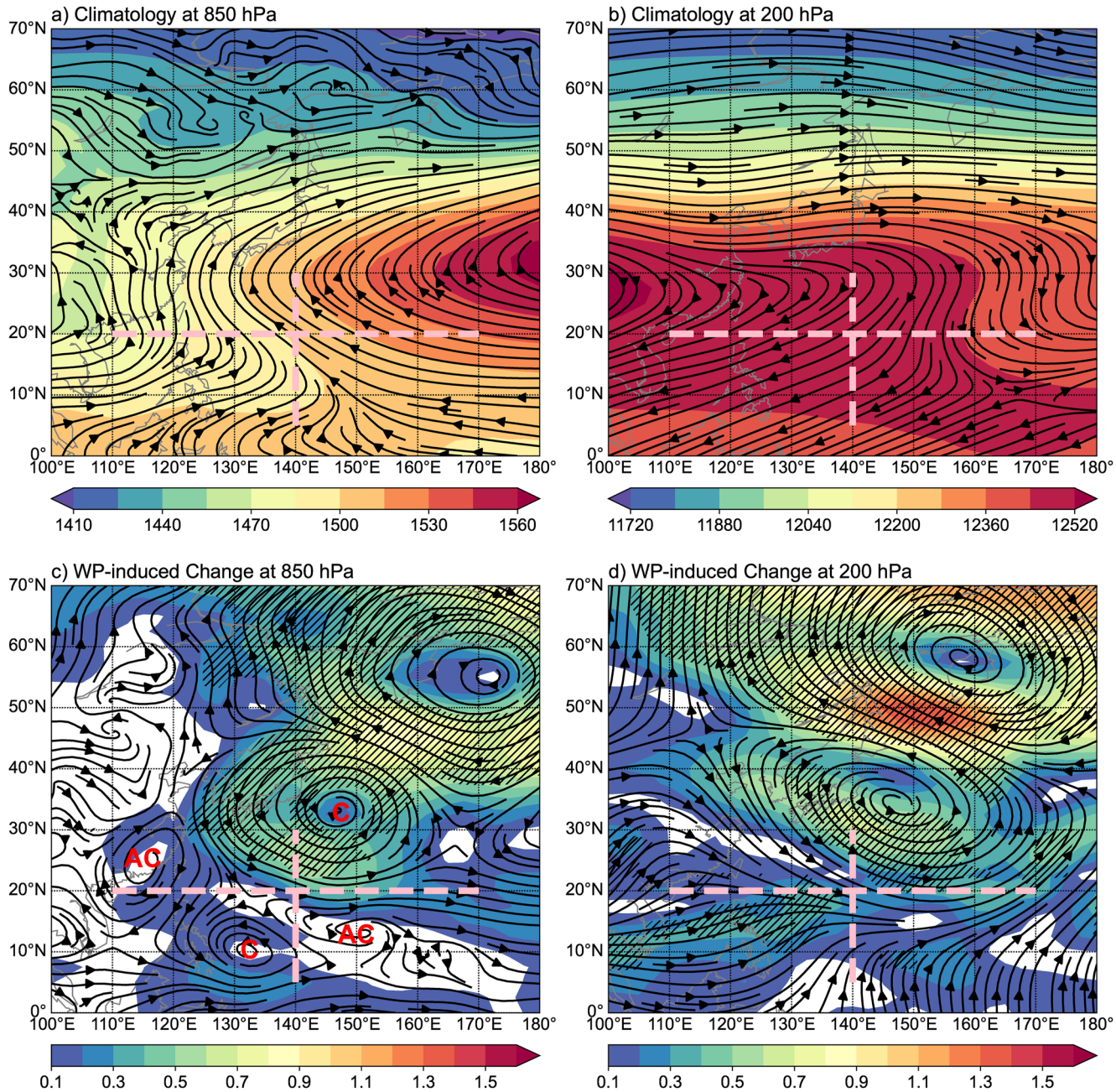

Figure 4. (a, b) Climatological (1982–2021) geopotential heights and streamlines over the WNP at (a) 850 hPa and (b) 200 hPa. (c, d) Regressions of (c) 850-hPa and (d) 200-hPa streamlines over the WNP onto the WP index, as well as their magnitudes. The pink dashed lines denote the four WNP quadrants. "C" and "AC" refer to anomalous cyclonic and anticyclonic circulations, respectively. Hatched areas denote regressions of wind anomalies significant at the 0.05 level.

5. Discussion

As previously noted, WNP RI magnitude is less influenced by changes in low-level relative vorticity on interannual timescales. To verify this observation, we apply 6-hourly STIP data from 1990 to 2020 to investigate potential contributors to RI occurrence and RI magnitude on synoptic timescales. There are a total of 1,451 RI events and 15,959 non-RI events (ΔV_{24} < 30 kt) in 6-hr intervals. Statistically speaking, the occurrence of RI events is associated with significantly larger MPI, TCHP, 700–500-hPa relative humidity, 850-hPa relative vorticity and 200-hPa divergence and significantly smaller 850–200-hPa VWS than that of non-RI events (Figure S2 in Supporting Information S1), consistent with previous studies (e.g., Fudeyasu et al., 2018; Knaff et al., 2018;

Shu et al., 2012). However, when only considering RI events, not all of the six environmental variables show significant relationships with RI magnitude (Figure S3 in Supporting Information S1). RI magnitude is significantly correlated with TCHP, 200-hPa divergence and 850–200-hPa VWS, although corresponding correlations are quite small ($r < 0.10$). By contrast, MPI, 700–500-hPa relative humidity and 850-hPa relative vorticity have insignificant correlations with RI magnitude.

6. Summary

The interannual variability of WNP RI magnitude is investigated in this study. There is only a weak correlation between RI number and RI magnitude during JASON from 1982 to 2020. WNP RI magnitude is significantly correlated with the WP teleconnection, regardless of whether the influence of ENSO or the AAO is considered. On average, basinwide RI magnitude is significantly larger (smaller) in positive (negative) phases of the WP. During a positive WP, changes in RI occurrence exhibit a south-north dipolar pattern, with comparable increases and decreases in magnitude, respectively. By contrast, there is a southwest-northeast dipolar structure west of 140°E in RI magnitude changes, with significant RI magnitude increases over the SWWNP (south of 20°N, west of 140°E) and weak decreases in RI magnitude over the NWNP (north of 20°N).

The influence of the WP teleconnection on RI magnitude can be explained by changes in large-scale environmental variables. 850–200-hPa VWS likely plays a more important role in influencing RI magnitude over most of the WNP than do other variables (e.g., MPI, TCHP, 700-500-hPa relative humidity, 850-hPa relative vorticity and 200-hPa divergence). During a positive WP, VWS is significantly reduced over the SWWNP, including the SCS and the area east of the Philippines, inducing strong RI magnitude increases. Only slight and insignificant VWS increases occur over most of the NWNP, leading to weak decreases in RI magnitude. By comparison, during a positive WP, RI occurrence is significantly enhanced over the SWWNP, which is driven by the joint influences of increased relative vorticity and VWS. RI occurrence is significantly suppressed over the NWWNP (north of 20°N, west of 140°E), predominately because of decreased relative vorticity. These changes in 850–200-hPa VWS and 850-hPa relative vorticity can be further linked to WP-induced circulation anomalies at lower and upper levels.

Song et al. (2020) reported a basinwide increasing trend in RI magnitude over the WNP, which was primarily driven by the warming ocean (e.g., increasing SSTs and TCHPs). Li et al. (2023) compared the RI magnitude anomalies over the WNP in two years: 1998 and 2010. The warming ocean coupled with an unstable atmosphere led to the high RI magnitude in 1998, while reduced low-level relative vorticity induced the low RI magnitude in 2010. By comparison, our study focuses on changes in WNP RI magnitude on interannual timescales. We find that VWS plays a more important role in modulating RI magnitude than other environmental conditions, such as SST, TCHP and low-level vorticity. Strong VWS can induce vertical tilt in the TC structure, suppressing TC intensification. It is likely that RI occurs when thermodynamic conditions are favorable (e.g., high SST, large TCHP, etc.), while its magnitude is controlled by dynamic conditions, particularly VWS. Our study also highlights that changes in RI occurrence and RI magnitude over the WNP on both interannual and synoptic timescales may be driven by different large-scale factors. RI magnitude tends to be less influenced by low-level environmental relative vorticity than RI occurrence.

Our results are mainly obtained through statistical analysis and should be verified by numerical sensitivity tests. In addition, the impacts of different environmental conditions on RI magnitude should be examined and compared with those for RI occurrence.

Data Availability Statement

Best track data is obtained from Knapp et al. (2018). HadISST data is available at: https://www.metoffice.gov.uk/hadobs/hadisst/data/download.html. ERA5 data is retrieved from Hersbach et al. (2017). ORAS5 data is available at Copernicus Climate Change Service (2021). The monthly timeseries of the Niño-3.4 SST anomaly and the Antarctic Oscillation (AAO) index are obtained from: https://psl.noaa.gov/data/climateindices/. STIPS developmental data is available at http://rammb.cira.colostate.edu/research/tropical_cyclones/ships/.

Acknowledgments
This work was funded by the National Natural Science Foundation of China (61827901, 42175007, 41905001 and 42192554) and the Meteorological Research Program of Guangxi Province of China (2023ZL04). Klotzbach would like to acknowledge financial support from the G. Unger Vetlesen Foundation.

References

Balaguru, K., Foltz, G. R., & Leung, L. R. (2018). Increasing magnitude of hurricane rapid intensification in the central and eastern tropical Atlantic. *Geophysical Research Letters*, *45*(9), 4238–4247. https://doi.org/10.1029/2018gl077597

Barnston, A. G., & Livezey, R. E. (1987). Classification, seasonality and persistence of low-frequency atmosphere circulation patterns. *Monthly Weather Review*, *115*(6), 1083–1125. https://doi.org/10.1175/1520-0493(1987)115<1083:csapol>2.0.co;2

Choi, K.-S., & Moon, I.-J. (2012). Influence of the Western Pacific teleconnection pattern on western North Pacific tropical cyclone activity. *Dynamics of Atmospheres and Oceans*, *57*, 1–16. https://doi.org/10.1016/j.dynatmoce.2012.04.002

Copernicus Climate Change Service. (2021). ORAS5 global ocean reanalysis monthly data from 1958 to present [Dataset]. Copernicus Climate Change Service (C3S) Climate Data Store (CDS). https://doi.org/10.24381/cds.67e8eeb7

DeMaria, M., Franklin, J. L., Onderlinde, M. J., & Kaplan, J. (2021). Operational forecasting of tropical cyclone rapid intensification at the National Hurricane Center. *Atmosphere*, *12*(6), 683. https://doi.org/10.3390/atmos12060683

DeMaria, M., Mainelli, M., Shay, L. K., Knaff, J. A., & Kaplan, J. (2005). Further improvements to the statistical Hurricane intensity prediction scheme (SHIPS). *Weather and Forecasting*, *20*(4), 531–543. https://doi.org/10.1175/waf862.1

Emanuel, K. A. (1988). The maximum intensity of hurricanes. *Journal of the Atmospheric Sciences*, *45*(7), 1143–1155. https://doi.org/10.1175/1520-0469(1988)045<1143:tmioh>2.0.co;2

Fudeyasu, H., Ito, K., & Miyamoto, Y. (2018). Characteristics of tropical cyclone rapid intensification over the western North Pacific. *Journal of Climate*, *31*(21), 8917–8930. https://doi.org/10.1175/jcli-d-17-0653.1

Ge, X., Shi, D., & Guan, L. (2018). Monthly variations of tropical cyclone rapid intensification ratio in the western North Pacific. *Atmospheric Science Letters*, *9*(4), e814. https://doi.org/10.1002/asl.814

Guo, Y.-P., & Tan, Z.-M. (2021). Influence of different ENSO types on tropical cyclone rapid intensification over the western North Pacific. *Journal of Geophysical Research*, *126*(11), e2020JD033059. https://doi.org/10.1029/2020jd033059

Hendricks, E. A., Peng, M. S., Fu, B., & Li, T. (2010). Quantifying environmental control on tropical cyclone intensity change. *Monthly Weather Review*, *138*(8), 3243–3271. https://doi.org/10.1175/2010mwr3185.1

Hersbach, H., Bell, B., Berrisford, P., Hirahara, S., Horányi, A., Muñoz-Sabater, J., et al. (2017). Complete ERA5 from 1940: Fifth generation of ECMWF atmospheric reanalyses of the global climate [Dataset]. Copernicus Climate Change Service (C3S) Data Store (CDS). https://doi.org/10.24381/cds.143582cf

Hong, J., & Wu, Q. (2021). Modulation of global sea surface temperature on tropical cyclone rapid intensification frequency. *Environmental Research Communications*, *3*(4), 041001. https://doi.org/10.1088/2515-7620/abf39b

Kaplan, J., & DeMaria, M. (2003). Large-scale characteristics of rapidly intensifying tropical cyclones in the North Atlantic basin. *Weather and Forecasting*, *18*(6), 1093–1108. https://doi.org/10.1175/1520-0434(2003)018<1093:lcorit>2.0.co;2

Kaplan, J., DeMaria, M., & Knaff, J. A. (2010). A revised tropical cyclone rapid intensification index for the Atlantic and east Pacific basins. *Weather and Forecasting*, *25*(1), 220–241. https://doi.org/10.1175/2009waf2222280.1

Knaff, A., Sampson, C. R., & DeMaria, M. (2005). An operational statistical typhoon intensity prediction scheme for the western North Pacific. *Weather and Forecasting*, *20*(4), 688–699. https://doi.org/10.1175/waf863.1

Knaff, J. A., Sampson, C. R., & Musgrave, K. D. (2018). An operational rapid intensification prediction aid for the western North Pacific. *Weather and Forecasting*, *33*(3), 799–811. https://doi.org/10.1175/waf-d-18-0012.1

Knapp, K. R., Diamond, H. J., Kossin, J. P., Kruk, M. C., & Schreck, C. J. (2018). International Best Track Archive for Climate Stewardship (IBTrACS) project, version 4 [Dataset]. NOAA National Centers for Environmental Information. https://doi.org/10.25921/82ty-9e16

Lee, C. Y., Tippett, M. K., Sobel, A. H., & Camargo, S. J. (2016). Rapid intensification and the bimodal distribution of tropical cyclone intensity. *Nature Communications*, *7*(1), 10625. https://doi.org/10.1038/ncomms10625

Li, Y., Zhan, R., & Zhao, J. (2023). What caused the salient difference in rapid intensification magnitudes of Northwest Pacific tropical cyclones between 1998 and 2010? *Atmospheric Research*, *285*, 106654. https://doi.org/10.1016/j.atmosres.2023.106654

Moon, I.-J., Kim, S.-H., & Chan, J. C. L. (2019). Climate change and tropical cyclone trend. *Nature*, *570*(7759), E3–E5. https://doi.org/10.1038/s41586-019-1222-3

Rayner, N. A., Parker, D. E., Horton, E. B., Folland, C. K., Alexander, L. V., Rowell, D. P., et al. (2003). Global analyses of sea surface temperature, sea ice, and night marine air temperature since the late nineteenth century. *Journal of Geophysical Research*, *108*(D14), 4407. https://doi.org/10.1029/2002jd002670

Shimada, U., Yamaguchi, M., & Nishimura, S. (2020). Is the number of tropical cyclone rapid intensification events in the western North Pacific increasing? *SOLA*, *16*(0), 1–5. https://doi.org/10.2151/sola.2020-001

Shu, S., Ming, J., & Chi, P. (2012). Large-scale characteristics and probability of rapidly intensifying tropical cyclones in the western North Pacific basin. *Weather and Forecasting*, *27*(2), 411–423. https://doi.org/10.1175/waf-d-11-00042.1

Song, J., Duan, Y., & Klotzbach, P. J. (2020). Increasing trend in rapid intensification magnitude of tropical cyclones over the western North Pacific. *Environmental Research Letters*, *15*(8), 084043. https://doi.org/10.1088/1748-9326/ab9140

Song, J., Klotzbach, P. J., Dai, Y., & Duan, Y. (2022). Does the Antarctic Oscillation modulate tropical cyclone rapid intensification over the western North Pacific? *Environmental Research Letters*, *17*(6), 064040. https://doi.org/10.1088/1748-9326/ac73ab

Trenberth, K. E. (1984). Some effects of finite sample size and persistence on meteorological statistics. Part I: Autocorrelations. *Monthly Weather Review*, *112*(12), 2359–2368. https://doi.org/10.1175/1520-0493(1984)112<2359:seofss>2.0.co;2

Wallace, J. M., & Gutzler, D. S. (1981). Teleconnections in the geopotential height field during the Northern Hemisphere winter. *Monthly Weather Review*, *109*(4), 784–812. https://doi.org/10.1175/1520-0493(1981)109<0784:titghf>2.0.co;2

Wang, B., & Zhou, X. (2008). Climate variation and prediction of rapid intensification in tropical cyclones in the western North Pacific. *Meteorology and Atmospheric Physics*, *99*(1–2), 1–16. https://doi.org/10.1007/s00703-006-0238-z

Zuo, H., Balmaseda, M. A., Tietsche, S., Mogensen, K., & Mayer, M. (2019). The ECMWF operational ensemble reanalysis-analysis system for ocean and sea-ice: A description of the system and assessment. *Ocean Science*, *15*(3), 779–808. https://doi.org/10.5194/os-15-779-2019